Nuclear Engineering and Technology xxx (xxxx) xxx

Contents lists available at ScienceDirect

Nuclear Engineering and Technology

journal homepage: www.elsevier.com/locate/net

Original Article

Design optimization of GaN diode with p-GaN multi-well structure for high-efficiency betavoltaic cell

Young Jun Yoon [a], Jae Sang Lee [a], In Man Kang [b], Jung-Hee Lee [b], Dong-Seok Kim [a, *]

[a] Korea Multi-purpose Accelerator Complex, Korea Atomic Energy Research Institute, Gyeogju, 38180, Republic of Korea
[b] School of Electronic and Electrical Engineering, Kyungpook National University, Daegu, 41566, Republic of Korea

ARTICLE INFO

Article history:
Received 18 June 2020
Received in revised form
27 August 2020
Accepted 14 September 2020
Available online xxx

Keywords:
GaN
Betavoltaic cell
Multi-well structure
High-efficiency
TCAD simulation

ABSTRACT

In this work, we propose and design a GaN-based diode with a p-doped GaN (p-GaN) multi-well structure for high efficiency betavoltaic (BV) cells. The short-circuit current density (J_{SC}) and open-circuit voltage (V_{OC}) of the devices were investigated with variations of parameters such as the doping concentration, height, width of the p-GaN well region, well-to-well gap, and number of well regions. The J_{SC} of the device was significantly improved by a wider depletion area, which was obtained by applying the multi-well structure. The optimized device achieved a higher output power density by 8.6% than that of the conventional diode due to the enhancement of J_{SC}. The proposed device structure showed a high potential for a high efficiency BV cell candidate.

1. Introduction

Betavoltaic (BV) cells have been studied as an attractive candidate for low-power micro-battery applications where a long life of the energy source is needed, such as implantable medical devices as well as military and space applications [1,2]. A wide-band gap semiconductor GaN has been used for development of high efficiency BV cells because GaN material has merits in terms of performance and radiation hardness compared to Si material [3,4].

However, GaN BV cells based on Schottky diodes and vertically stacked p-(i)-n diodes exhibited a poor power conversion efficiency because of problems including charge generation and collection efficiency [5–11]. In order to utilize the GaN-based BV cell as a micro-battery, the efficiency of the BV cells should be improved by the design of the diode structure. Several researchers presented and designed novel structures of the BV cells to improve the charge generation and collection [12,13]. Various diode structures can be fabricated for GaN-based BV cells with a high power conversion efficiency by considering the growth and implantation technologies. It is important to maximize the width of depletion regions and reduce the trap-assisted recombination in the diode for improving a power conversion efficiency. Especially, the depletion regions directly related to the charge collection because electron-hole pairs (EHPs) formed in the depletion region converted to electric current [14].

In this work, we proposed a GaN-based diode with a p-doped GaN (p-GaN) multi-well structure for high efficiency BV cells. The multi-well structure can efficiently increase the depletion width because of the crossed PN junction. The device's structure was designed using a three-dimensional (3-D) technology computer-aided design (TCAD) simulator to evaluate the short-circuit current density (J_{SC}) and an open-circuit voltage (V_{OC}), associated with the power conversion efficiency. Reverse current characteristics under electron-beam (e-beam) irradiation were analyzed with variations in parameters of the p-GaN well region such as the doping concentration ($D_{p\text{-}GaN}$), height ($H_{p\text{-}GaN}$), and width ($W_{p\text{-}GaN}$) in single well structure. After optimizing the single well structure, the effects of the multi-well structure on the J_{SC} and V_{OC} were investigated in term of a well-to-well gap and the number of well regions. The output power density of the optimized and conventional diode-based BV cells was compared to verify the potential for BV cell with a high efficiency.

2. Device structure and simulation method

Fig. 1 shows the 3-D schematic diagrams of the proposed diode with the p-GaN single- and multi-well structures. The device

* Corresponding author.
E-mail address: dongseokkim@kaeri.re.kr (D.-S. Kim).

https://doi.org/10.1016/j.net.2020.09.014

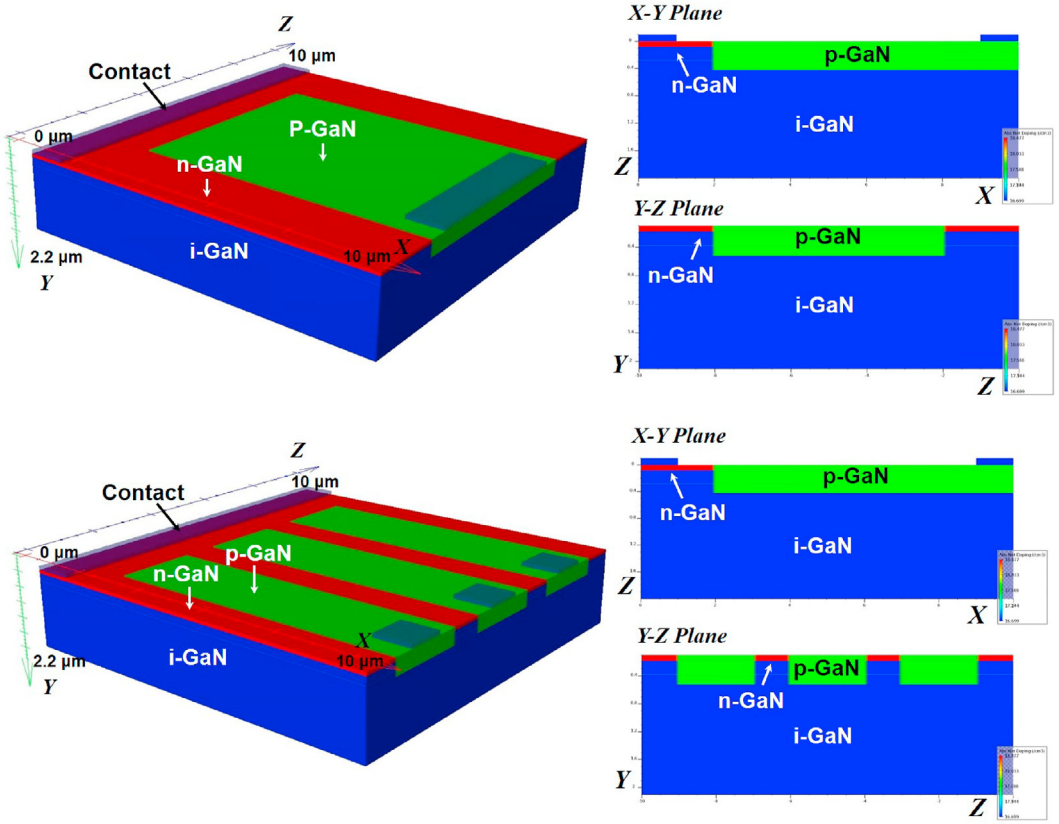

Fig. 1. 3-D schematic and cross-sectional schematic diagrams of the proposed diode structure. (Top) p-GaN single well and (Bottom) p-GaN multi-well structures. A total size of the device is 10 μm × 10 μm.

consists of n-doped GaN (n-GaN) and p-GaN well regions on an intrinsic or undoped GaN (i-GaN) layer. The device can be fabricated using metal-organic chemical vapor deposition (MOCVD) and implantation processes. First, the i-GaN and n-GaN layers are sequentially grown on a substrate using MOCVD equipment. After the growth process, Mg ions are selectively implanted to form the p-GaN well region. The implantation technology is used to design GaN-based electronic and photonic devices [15,16]. The doping concentrations of i-GaN and n-GaN layers ($D_{\text{i-GaN}}$ and $D_{\text{n-GaN}}$) are n-type 5 × 10^{16} cm^{-3} and 5 × 10^{18} cm^{-3}, respectively. The highly doped n-GaN layer is designed for a low ohmic contact resistance, which affects conversion efficiency because the limit of electron movements is caused by a high contact resistance. The height of the n-GaN layer ($H_{\text{n-GaN}}$) is 80 nm. Contact resistances for the n-GaN and p-GaN regions are set as 1 × 10^{-4} Ω cm^2 assuming ohmic contact. The p-GaN well region, formed by using the implantation, is a key parameter in the proposed device because the depletion area between the n-GaN and p-GaN regions or i-GaN and p-GaN regions are changed by the parameters of p-GaN such as the doping concentration ($D_{\text{p-GaN}}$), height ($H_{\text{p-GaN}}$), and width ($W_{\text{p-GaN}}$). Thus, the effects of these parameters on the performance were verified to optimize the proposed device with a total size of 10 μm × 10 μm. The total width of p-GaN regions in the multi-well structure ($W_{\text{m,p-GaN}}$) was designed by considering the device's size. The current performances employing the e-beam irradiation were obtained and analyzed using the 3-D TCAD simulator [17]. In the e-beam irradiation model, the rate of the EHPs generation is determined by the e-beam energy and the energy loss as a function of the depth. The energy in the used e-beam irradiation was 17 keV as an average energy of the Ni-63 radioisotope [18]. The Ni-63 radioisotope has recently been seen as a promising source of BV cells due to the merits including a long half-life over 100 years. The dissipated energy and penetration distance in the GaN material are determined by the function derived from the Bohr-Bethe energy-loss relation [19]. The threshold energy required for forming the EHPs in the GaN material was 8.9 eV. The variation of dissipated energy as a function of depth affected EHPs generation rate. The absorption rate vs. penetration depth for 17 keV e-beam irradiation is shown in Fig. 2. A 17 keV e-beam is penetrated up to a depth of 1 μm and exhibited a maximum absorption rate in a depth of 300 nm in GaN material. The output power density of the proposed devices was evaluated by comparing with that of the conventional devices. The heights of the i-GaN layer ($H_{\text{i-GaN}}$) and $H_{\text{p-GaN}}$ in the conventional

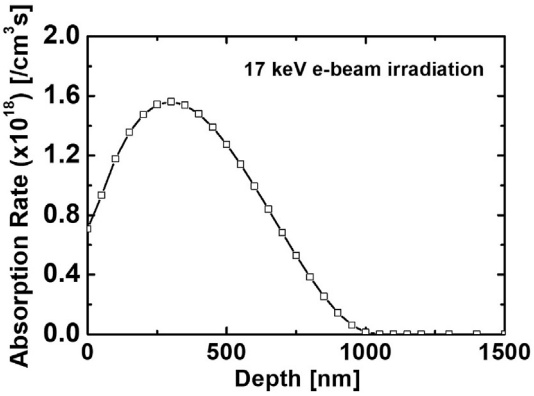

Fig. 2. Absorption rate vs. penetration depth in GaN material for 17 keV e-beam irradiation.

device were 500 nm and 200 nm, respectively. The heights of these devices were designed considering the penetration depth of the 17 keV e-beam, and were similar to the fabricated BV cell structure [8,11]. The doping concentrations of each layer in the conventional device are equal to the proposed device. In the simulation, the carrier generation-recombination and low-field mobility models were employed because the models affect the current characteristics of GaN diodes. In the models, bandgap energy, minority carrier lifetime, effective mass, and permittivity for GaN material were defined as 3.43 eV, 10^{-9} s, 0.23($\times$ m_0), and 8.9, respectively. In addition, we applied traps existing in GaN materials to reflect the trap-assisted recombination effects. The donor and acceptor traps were related by Ga- and N-vacancy (V_{Ga} and V_N) and were located in E_C-0.23 eV, E_C-0.6 eV and E_V-0.92 eV, respectively [20–22]. The density of the applied traps was 9.5 $\times$ 10^{14} cm^{-3}, 3.2 $\times$ 10^{14} cm^{-3}, and 6.6 $\times$ 10^{14} cm^{-3}, respectively.

3. Results and discussion

Fig. 3 shows the reverse characteristics of the proposed device without and with the 17 keV e-beam irradiation. The device was designed as a p-GaN single-well structure with a $D_{p\text{-}GaN}$ of 1 $\times$ 10^{17} cm^{-3}, $W_{p\text{-}GaN}$ of 6 μm, and $H_{p\text{-}GaN}$ of 350 nm. The reverse current in the device was increased due to the EHPs generated by the e-beam irradiation. The device exhibited a J_{SC} of −10.1 μA/cm^2 and a V_{OC} of 2.41 V. J_{SC} and V_{OC} are defined as a current density at zero voltage and a voltage when a current density is zero. The J_{SC} is affected by both the generation and collection of charges. The generated electrons and holes were moved by the electric field in the depletion area formed under and beside the p-GaN well region. The J_{SC} of the device can be increased by extending the depletion area. Because the depletion is affected by the $D_{p\text{-}GaN}$ and dimensions of the p-GaN well region, we investigated the reverse current characteristics according to the change of the p-GaN well structure.

Fig. 4 shows the variations in the reverse current density of the devices depending on the $D_{p\text{-}GaN}$ when the e-beam was irradiated. The device was designed as a p-GaN single-well structure with a $W_{p\text{-}GaN}$ of 6 μm and a $H_{p\text{-}GaN}$ of 350 nm. In the case of a $D_{p\text{-}GaN}$ of 1 $\times$ 10^{17} cm^{-3}, it exhibited the highest J_{SC}, although the reverse current density in a voltage ranging from −1 V to −6 V as the $D_{p\text{-}GaN}$ increased. This result indicated that the depletion region was maximized in the case of a $D_{p\text{-}GaN}$ of 1 $\times$ 10^{17} cm^{-3}. We determined

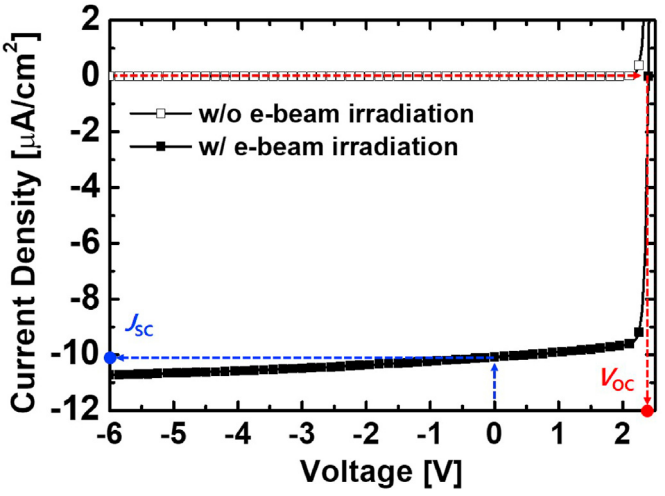

Fig. 3. Reverse characteristics of the proposed diode without and with the e-beam irradiation. $D_{p\text{-}GaN}$, $H_{p\text{-}GaN}$, and $W_{p\text{-}GaN}$ of the single well structure are 1 $\times$ 10^{17} cm^{-3}, 350 nm, and 6 μm, respectively.

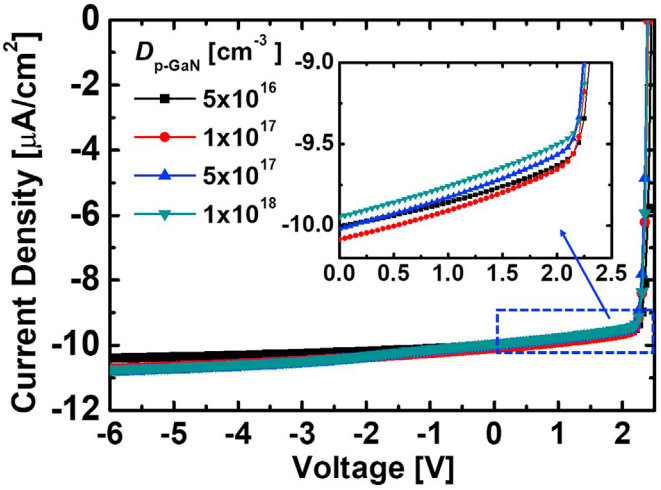

Fig. 4. Effects of a $D_{p\text{-}GaN}$ on reverse current density under the e-beam irradiation of the proposed devices with the single p-GaN well region. $H_{p\text{-}GaN}$ and $W_{p\text{-}GaN}$ of the single well structure are fixed as 350 nm and 6 μm, respectively.

that the optimum $D_{p\text{-}GaN}$ was 1 $\times$ 10^{17} cm^{-3} because a high J_{SC} influences an improved output power density. The effects of the $H_{p\text{-}GaN}$ and $W_{p\text{-}GaN}$ on the reverse current density of the device were verified in the case of a $D_{p\text{-}GaN}$ of 1 $\times$ 10^{17} cm^{-3}. The variation of the reverse current density according to the $H_{p\text{-}GaN}$ is shown in Fig. 5(a). As the $H_{p\text{-}GaN}$ increased from 140 nm to 420 nm, the reverse current density dramatically rose because the location of the depletion area under the p-GaN region matched the penetration depth range with a high absorption rate. In the case of a $H_{p\text{-}GaN}$ over 420 nm, the reverse current density decreased due to a mismatch between the location of the depletion area and the depth of the absorption rate. As shown in Fig. 5(b), the device exhibited the highest J_{SC} when the $H_{p\text{-}GaN}$ was 420 nm in the case of a $D_{p\text{-}GaN}$ of 1 $\times$ 10^{17} cm^{-3}. Because the V_{OC} of the device was almost unaffected by $H_{p\text{-}GaN}$, J_{SC} was the dominant factor in determining the output power density. When the $D_{p\text{-}GaN}$ changed to 5 $\times$ 10^{17} cm^{-3}, the optimum point of $H_{p\text{-}GaN}$ was also affected by the variation of the depletion area. In the case of a $D_{p\text{-}GaN}$ of 5 $\times$ 10^{17} cm^{-3}, the device designed with a $H_{p\text{-}GaN}$ of 350 nm obtained the enhanced J_{CS}. This result shows that the relation between $D_{p\text{-}GaN}$ and $H_{p\text{-}GaN}$ must be considered in term of structure design.

Fig. 6 shows the variation in the reverse current density of the devices with a different $W_{p\text{-}GaN}$ under the e-beam irradiation. The reverse current density was significantly affected by the $W_{p\text{-}GaN}$. A wider $W_{p\text{-}GaN}$ improved the reverse current density because of the increase in the depletion area that formed between the p-GaN and i-GaN regions. This result indicated that the depletion area under p-GaN well regions is a dominant factor in determining the charge generation and collection. The device with the p-GaN multi-well structures obtained a higher J_{SC} than that of the device designed by the single well with a $W_{p\text{-}GaN}$ of 8 μm, although the total width of the multi-well structures was smaller ($W_{m,p\text{-}GaN}$:6 μm). The multi-well structure improved the charge generation and collection owing to the additionally extended depletion area. Thus, we analyzed the effects of a well-to-well gap and a number of well regions on the J_{SC} for optimizing the multi-well structure. The variation in the reverse current density of the device depending on the well-to-well gaps in the multi-well structure is shown in Fig. 7. When the well-to-well gap increased from 0.5 μm to 1.0 μm, the J_{SC} was enhanced by the extended depletion area. As the well-to-well gap increased over 1 μm, the J_{SC} was reduced by the decrease in the charge collection efficiency, which was caused by the increased in the highly doped region.

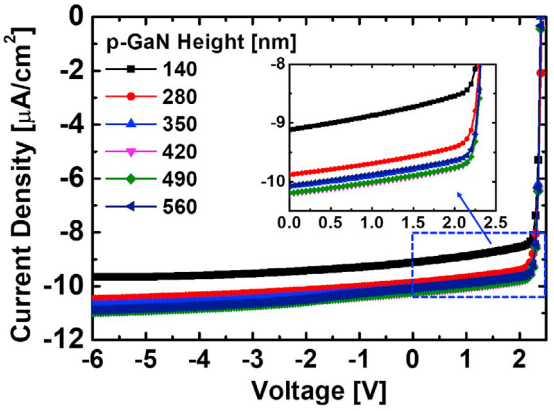

(a)

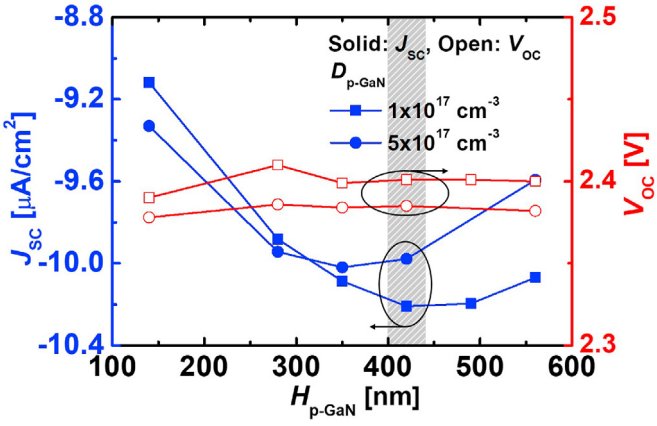

(b)

Fig. 5. (a) Effects of $H_{p\text{-}GaN}$ reverse current density under the e-beam irradiation of the proposed devices with single well region. (b) Variation in J_{SC} and V_{OC} as function of $H_{p\text{-}GaN}$. $D_{p\text{-}GaN}$ and $W_{p\text{-}GaN}$ of the single well structure are 1×10^{17} cm^{-3} and 6 μm, respectively.

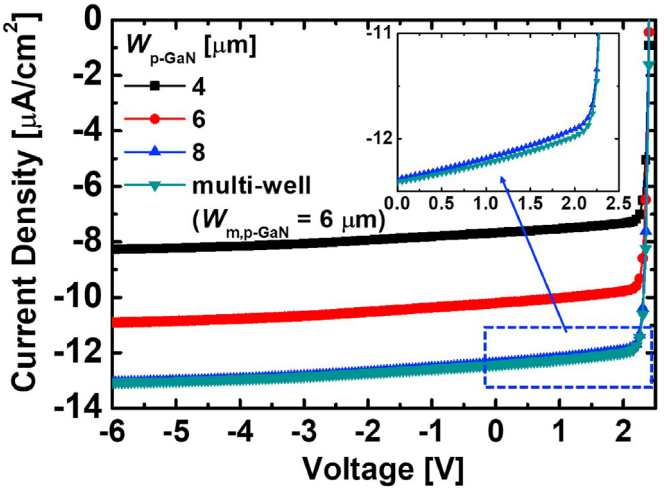

Fig. 6. Effects of $W_{p\text{-}GaN}$ on reverse current density under the e-beam irradiation of the proposed devices. $D_{p\text{-}GaN}$ and $H_{p\text{-}GaN}$ in the single well structure are 1×10^{17} cm^{-3} and 420 nm, respectively. A well-to-well gap in the three well regions is 1 μm.

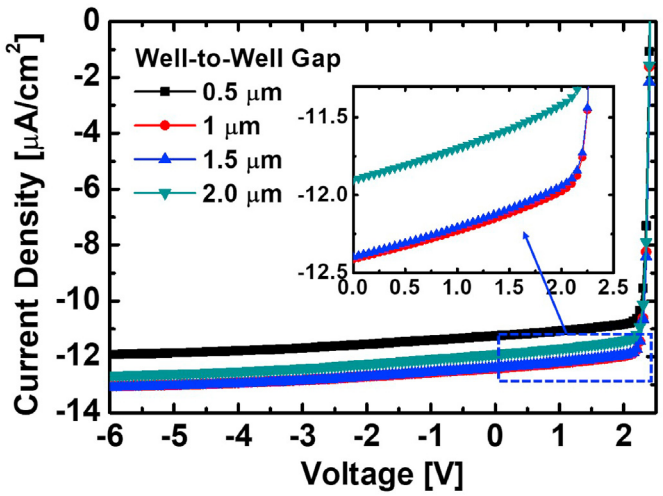

Fig. 7. Variation in reverse current density under the e-beam irradiation of the proposed devices with three well regions according to a well-to-well gap. $D_{p\text{-}GaN}$, $H_{p\text{-}GaN}$, and $W_{m,p\text{-}GaN}$ are 1×10^{17} cm^{-3}, 420 nm, and 6 μm, respectively.

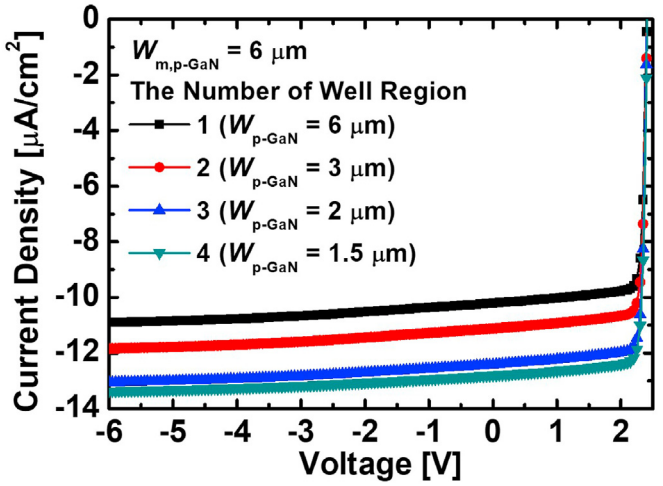

Fig. 8. Variation in reverse current density under the e-beam irradiation of the proposed devices according to the number of p-GaN well region. A $W_{m,p\text{-}GaN}$, a well-to-well gap, a $D_{p\text{-}GaN}$ and a $H_{p\text{-}GaN}$ in the multi-well structure are 6 μm, 1 μm, 1×10^{17} cm^{-3}, and 420 nm, respectively.

Fig. 8 shows the effects of the number of p-GaN well regions on the reverse current density of the devices under the e-beam irradiation. To analyze the impact of the number of well region, we determined that the $W_{m,p\text{-}GaN}$ and well-to well gap of all devices were 6 μm and 1 μm, respectively. In addition, the number of well regions increased up to 4 considering the device size of 10 μm × 10 μm, the $W_{m,p\text{-}GaN}$, and the well-to well gap. Many well regions improved the J_{SC} due to the extended depletion area side of the p-GaN well regions. The rise in the number of well regions increased the junction between the p-GaN and n-GaN regions, resulting in an extension of the depletion area side of the p-GaN well regions. The depletion area under the p-GaN well region was unchanged, although the number of wells increases because the $W_{m,p\text{-}GaN}$ of all devices was the same as 6 μm. As a result, the charge collection efficiency of the multi-well device was improved by the increased depletion area side of the p-GaN region. The multi-well

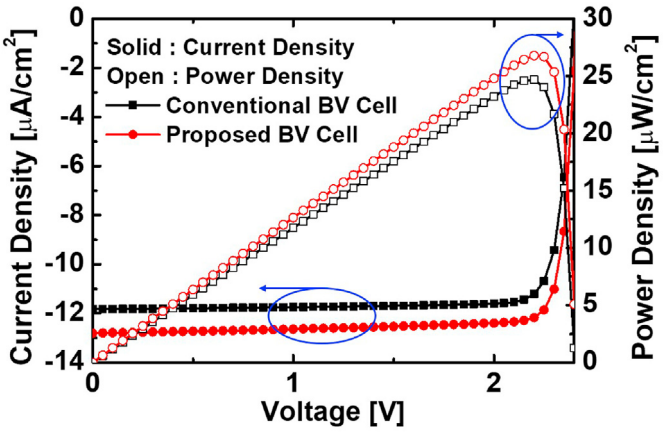

Fig. 9. Comparison of current and power density in conventional and proposed diodes under e-beam irradiation. The conventional diode structure was designed as the vertically stacked p-i-n structure with parameters ($D_{p\text{-}GaN} = 1 \times 10^{17}$ cm^{-3}, $D_{i\text{-}GaN} = 5 \times 10^{16}$ cm^{-3} $D_{n\text{-}GaN} = 5 \times 10^{18}$ cm^{-3}, $H_{p\text{-}GaN} = 200$ nm, and $H_{i\text{-}GaN} = 500$ nm).

device was optimized with the parameters including a $D_{p\text{-}GaN}$ of 1×10^{17} cm^{-3}, a $H_{p\text{-}GaN}$ of 420 nm, a $W_{m,p\text{-}GaN}$ of 6 μm, a well-to-well gap of 1 μm, and four well regions. The reverse current density and output power density of the optimized device were compared with that of the conventional device with vertically stacked p-i-n layers, as shown in Fig. 9. The proposed device obtained a higher output power density than that of the conventional device because the J_{SC} was improved by the extended depletion area. The output power density of both devices was affected by J_{SC} because of almost the same V_{OC}. This result indicated that the proposed structure achieved a high power conversion efficiency.

4. Conclusion

The GaN-based diode with the p-GaN multi-well regions was proposed and designed for a high efficiency BV cell. The effects of geometric parameters such as the $D_{p\text{-}GaN}$, $H_{p\text{-}GaN}$, $W_{p\text{-}GaN}$, well-to-well gap, and number of well regions on J_{SC} and V_{OC} were analyzed to optimize the structure. The optimized device achieved a higher J_{SC} than that of the conventional device because of the extended depletion area. The output power density of the optimized device increased by 8.6% compared to the conventional device. This resulted in an improved output power density. These results demonstrate the proposed device has a high potential for BV applications.

Declaration of competing interest

The authors declare that they have no known competing financial interests or personal relationships that could have appeared to influence the work reported in this paper.

Acknowledgments

This work was supported by the National Research Foundation of Korea (NRF) grant (No. 2018M2A2B3A01072437) funded by the Korea government-MSIT (Ministry of Science and ICT).

References

[1] L.C. Olsen, P. Cabauy, B.J. Elkind, Phys. Today 35 (2012) 35.
[2] M.G. Spencer, T. Alam, Appl. Phys. Rev. 6 (2019), 031305.
[3] A. Ionascut-Nedelcescu, C. Carlone, A. Houdayer, H.J. vol Bardeleben, J.-L. Cantin, S. Raymond, IEEE Trans. Nucl. Sci. 49 (2002) 2733.
[4] S.I. Maximenko, J.E. Moore, C.A. Affouda, P.P. Jenkins, Sci. Rep. 9 (2019), 10892.
[5] M. Lu, G.-G. Zhang, K. Fu, G.-H. Yu, D. Su, J.-F. Hu, Energy Convers. Manag. 52 (2011) 1955.
[6] Z.J. Cheng, H.S. San, Z.H. Feng, B. Liu, X.Y. Chen, Electron. Lett. 47 (2011) 720.
[7] Z. Cheng, X. Chen, H. San, Z. Feng, B. Liu, J. Micromech. Microeng. 22 (2012), 074011.
[8] C.E. Munson, M. Arif, J. Streque, S. Belahsene, A. Martinez, A. Ramdane, Y.E. Gmili, J.-P. Salvestrini, P.L. Voss, A. Ougazzaden, J. Appl. Phys. 118 (2015), 105101.
[9] M.R. Khan, J.R. Smith, R.P. Tompkins, S. Kelley, M. Litz, J. Russo, J. Leathersich, F. Shahedipour-Sandvik, K.A. Jones, A. Iliadis, Solid State Electron. 136 (2017) 24.
[10] N.A. Kuruoglu, O. Ozdemir, K. Bozkurt, Thin Solid Films 636 (2017) 746.
[11] S. Aydin, E. Kam, Int. J. Energy Res. 43 (2019) 8725.
[12] K. Hogan, M. Litz, F. Shahedipour-Sandvik, Appl. Radiat. Isot. 82 (2019) 119.
[13] J.W. Murphy, L.F. Voss, C.D. Frye, Q. Shao, K. Kazkaz, M.A. Stoyer, R.A. Henderson, R.J. Nikolic, AIP Adv. 9 (2019), 065208.
[14] M. Wu, J. Zhang, AIP Adv. 9 (2019), 075124.
[15] D. Ji, M.A. Laurent, A. Agarwal, W. Li, S. Mandal, S. Keller, S. Chowdhury, IEEE Trans. Electron. Dev. 64 (2017) 805.
[16] S.J. Pearton, C.B. Vartuli, Appl. Phys. Lett. 67 (1995) 1435.
[17] Atlas User's Manual (Silvaco International Inc., Santa Clara, CA).
[18] H. San, S. Yao, X. Wang, Z. Cheng, X. Chen, Appl. Radiat. Isot. 80 (2013) 17.
[19] T.E. Everhart, P.H. Hoff, J. Appl. Phys. 42 (1971) 5837.
[20] H.K. Cho, C.S. Kim, C.-H. Hong, J. Appl. Phys. 94 (2003) 1485.
[21] A.Y. Polyakov, I.-H. Lee, N.B. Smirnov, A.V. Govorkov, E.A. Kozhukhova, S.J. Pearton, J. Appl. Phys. 109 (2011), 123701.
[22] E. Challeja, F.J. Sanchez, D. Basak, M.A. Sanchez-Garcia, E. Munoz, I. Izpura, F. Calle, J.M.G. Tijero, J.L. Sanchez-Rojas, B. Beaumont, P. Lorenzini, P. Gibart, Phys. Rev. B 55 (1997) 4689.